Applied Physics Letters ARTICLE pubs.aip.org/aip/apl

Depth profile of trap concentration induced by heavy ion irradiation in 4H-SiC Schottky barrier diode

Cite as: Appl. Phys. Lett. **127**, 023507 (2025); doi: 10.1063/5.0266534
Submitted: 19 February 2025 · Accepted: 30 June 2025 ·
Published Online: 18 July 2025

Xueqiang Yu, Xiaodong Xu,[a] Hao Jiang, Lei Wu, Fengkai Liu, Weiqi Li, Zhongli Liu, Hongbin Geng, Jianqun Yang, and Xingji Li[a]

AFFILIATIONS

Technology Innovation Center of Materials and Devices at Extreme Environment, School of Materials Science and Engineering, Harbin Institute of Technology, Harbin 150001, People's Republic of China

[a]**Authors to whom correspondence should be addressed:** xuxd@hit.edu.cn and lxj0218@hit.edu.cn

ABSTRACT

Displacement damage in silicon carbide (SiC) power devices induced by heavy ions severely limited their application in aerospace engineering, and the investigation of defect distribution in devices has consistently been a critical research focus. In this work, the degradation of capacitance performance in a 4H-SiC Schottky barrier diode (SBD) irradiated by heavy ions was explored. The capacitance–voltage (C–V) characterization reveals an evident decrease in the local carrier concentration of 4H-SiC SBD following the irradiation with three types of heavy ions. Deep level transient spectroscopy shows three traps at 0.63, 0.57, and 0.38 eV below the conduction band in the epitaxial layer, respectively. The depth profile of trap concentration in the space charge region was used to explain the degradation of the local carriers. Our results build the relationship between carrier removal effect and trap concentration, providing insights into the underlying mechanisms of displacement damage effects in 4H-SiC devices.

In recent years, lots of research has focused on 4H-SiC power devices for high-power, high-temperature, and radiation hardness applications due to their outstanding thermal conductivity, wide bandgap, and high breakdown field.[1–4] Benefiting from the faster switching speed and lower switching losses, the 4H-SiC Schottky barrier diode (SBD) is widely used in power switching applications, and it has demonstrated its application value in aerospace engineering.[5,6] However, electronic devices in spacecraft face various high-energy particle irradiation in the space environment. Various point defects induce displacement damage in semiconductors, which introduces a variety of deep energy levels in the bandgap for the semiconductor.[7–13] In general, any disturbance of lattice periodicity may give rise to energy levels in the bandgap, which leads to the compensation of donors or acceptors.[14] SiC devices have shown better radiation hardness due to the wide bandgap and higher displacement energies for both Si and C lattice atoms compared to silicon devices. The 4H-SiC power module, with its excellent total ionizing dose (TID) radiation resistance and high efficiency, is considered a candidate for applications in hard radiation environments.[15,16] However, defects may be unintentionally introduced by displacement damage dose (DDD), which can act as carrier generation–recombination centers to degrade device performance and reliability.[17–20]

As a method for detecting defects in semiconductors, deep level transient spectroscopy (DLTS) measurement has been widely used to characterize defects in devices. The energy levels of defects can be detected by monitoring the capacitance transients of a junction associated with carrier emission.[21–24] Double-correlated deep level transient spectroscopy (D-DLTS) has conventionally been used to characterize the depth profile of traps when the trap density shows a spatial distribution. However, the D-DLTS has a trade-off relationship between the depth resolution and the resolution in the carrier trap density due to the measurement principle, while the isothermal capacitance transient spectroscopy (ICTS) presented a good accuracy in characterizing traps with spatial distribution in the detection region.[25,26] To gain a deeper understanding of the impacts of defects on device properties, it is academically and technically important to investigate the density and depth profile of carrier traps.

Some deep levels in 4H-SiC served as the carrier killers for capturing and recombining carriers. The presence of carbon-related point defects in 4H-SiC, particularly carbon vacancies (V_C), acts as a major

cause for carrier recombination in devices.[27–30] V_C has been connected to deep levels measured by DLTS and labeled the $Z_{1/2}$ and $EH_{6/7}$ centers.[31,32] Previous studies observed the reduction of carrier concentration after irradiation with protons, electrons, heavy ions, and neutrons.[33–35] At present, research on the radiation effects for silicon carbide devices mainly focuses on the electrical performance degradation and defect property calculations of 4H-SiC, but studies have demonstrated that the inhomogeneous spatial distribution of defects in SBD contributes to localized degradation in carrier concentration[36,37] and an increase in the ideality factor (n) in the sub-threshold region.[38] The studies of defects in 4H-SiC, including energy levels, concentration, and distribution, are crucial to understanding the degradation of the carrier transport dynamics and the correlated device performances caused by displacement damage.

This work revealed the degradation of the capacitance characteristics of 4H-SiC SBD under irradiation by different heavy ions utilizing DLTS and ICTS. We presented the depth profile of trap concentration calculated within the space charge region. We clarified the distribution characteristics of trap concentration and carrier concentration located at the tail of the heavy ion radiation range. The deep energy levels induced by heavy ion irradiation in 4H SiC SBD were analyzed using DLTS technology, and the relationship between trap concentration and the degradation of carrier concentration is presented to demonstrate the electrical degradation of devices caused by heavy ion irradiation.

4H-SiC SBD was fabricated using 11 μm n-type epilayers (nitrogen-doped with 1.2×10^{15} cm^{-3}) grown on highly doped n-type substrates (150 μm), which were purchased from the 55th Research Institute of China Electronics Technology Group Corporation. A 40 nm thick titanium layer was evaporated on the epitaxial layer to form the Schottky contact, followed by the deposition of a 4 μm thick aluminum layer on the top of the titanium layer to serve as the anode of the SBD. Both the titanium layer and the aluminum layer deposited on the top Schottky are square shaped with an area of 1.80×1.80 mm^2 and the epitaxial and the substrate layer have an area of 2.05×2.05 mm^2. Full-area Ni/Ag (1.6 μm) Ohmic contacts were formed on the bottom of the substrate. The barrier heights of all samples are approximately 1.2 V, with leakage currents in the nA range at room temperature. The cross-sectional schematic of the 4H-SiC SBD is presented in Fig. 1(a).

All samples were irradiated in the EN-tandem accelerator at Peking University. The SBDs were irradiated by 12 MeV carbon (C), 18 MeV oxygen (O) and 18 MeV fluorine (F), respectively. The ion irradiation fluence rate during the experiment was 1×10^7 ions/cm^2·s and the ion fluences are 5×10^8, 1×10^9, 5×10^9, and 1×10^{11} ions/cm^2, respectively. All pins of the devices were grounded during irradiation. The forward current–voltage (I–V) plots capacitance–voltage (C–V) plots were measured at room temperature using a Keysight B1500A Semiconductor Device Parameter Analyzer.

Figure 1(b) presents the non-ionizing energy loss (NIEL) in 4H-SiC SBDs irradiated by 12 MeV C, 18 MeV O, and 18 MeV F. The NIEL was calculated using Extreme-environment Radiation Effect Technology Computer Aided Design (ERETCAD) software.[40] The NIEL in 4H-SiC SBD irradiated by heavy ions is mainly deposited in the tail of the ion range trajectory.

Figure 2 shows the plots of $1/C^2$ vs reverse voltage measured at various irradiation fluences for the 4H-SiC SBDs and the depth profile of free carrier concentration. The depth profiles of free carrier concentration can be derived using the following equation:

$$N_D(x) = \frac{2}{q\varepsilon\varepsilon_0 A^2 \left\{ d\left(1/C^2\right)/d(U_R) \right\}}. \quad (1)$$

The depth of depletion region in the epitaxial layer under bias voltage U_R is given by the following equation:

$$x(U_R) = \frac{\varepsilon\varepsilon_0 A}{C(U_R)}, \quad (2)$$

where N_D (x) is the carrier concentration at the depth (x) of the epitaxial layer, q is the elementary charge, ε_0 is the vacuum dielectric constant, ε is the electrical permittivity of 4H-SiC ($\varepsilon = 10.3$), A is the Schottky contact area, and C_R is the capacitance of the SBD in the reverse voltage.

As shown in Figs. 2(a)–2(c), all the C–V plots for the SBDs irradiated by heavy ions presented a region of anomalous degradation with a large difference. The anomalous decrease in capacitance with the increase in bias voltage when the SBDs were irradiated by heavy ions, which can be assigned to the cumulatively increasing concentration of ion-induced defects in the epitaxial layer. It is noteworthy that the degradation of C–V plots increased with the increase in irradiation fluence and the anomalous variation region shifted positively. The capacitance characteristics of all devices deteriorated severely when the irradiation fluence was 5×10^9 ions/cm^2. Figures 2(d)–2(f) present the depth profile of carrier concentration in the SBD at different irradiation fluences, indicating the net free carrier concentration removal effects and the disruption of the uniformity of carrier concentration in the device were caused by the deposition of heavy ions in the epitaxial layer. As a result, the degree of carrier concentration degradation caused by the irradiation of 12 MeV C, 18 MeV O, and 18 MeV F increased in sequence, and the degradation of local carrier concentration caused by heavy ion irradiation showed a diffusion trend with the increase in irradiation fluence. The free carriers were removed completely in the zone where the ions deposited when the ion fluence reached 5×10^9 ions/cm^2. It can be concluded that the observed anomalous doping profiles were caused by the inhomogeneous distribution of acceptor defects.

Generally, the carrier removal effect induced by radiation-introduced trap levels typically accompanies a decrease in the free carrier concentration within the epitaxial layer. This manifests electrically as a downward shift in the C–V curve, corresponding to an upward shift in the $1/C^2$–V curve. This implies that a stronger carrier removal effect results in a more pronounced decrease in device capacitance under the same bias voltage. When high-energy particles deposit energy within the device's epitaxial layer, the irregular distribution of trap levels throughout this layer leads to anomalous regions in the C–V characteristics. According to the relationship between depletion region depth and bias voltage given by Eqs. (1) and (2), the depletion depth at bias voltage U_R is related to the free carrier concentration. Consequently, at the same bias voltage, a reduction in carrier concentration within the epitaxial layer leads to a deeper depletion region. Crucially, the spatial location corresponding to the irregular trap distribution responsible for the anomalous region does not shift with increasing irradiation fluence. Therefore, as the irradiation fluence increases and the free carrier concentration in the epitaxial layer decreases, the anomalous region in the C–V curve shifts positively.

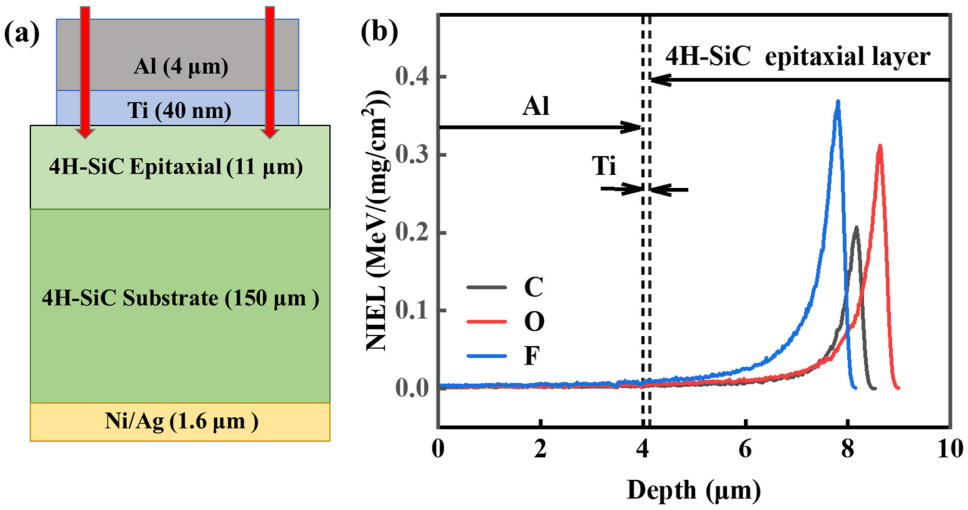

FIG. 1. (a) 2D schematic view for 4H-SiC SBD. (b) The depth of NIEL deposition in 4H SiC SBD under the irradiation of 12 MeV C, 18 MeV O, and 18 MeV F.

This phenomenon fundamentally reflects the mapping of the inhomogeneous spatial distribution of free carrier concentration onto the C–V curve.

In this work, we present schematic representations of the degradation in the semi-logarithmic current–voltage (I–V) characteristics of the devices under various ion irradiations. The semi-logarithmic I–V characteristics of the irradiated samples exhibit good linearity within the voltage range of 0.3–0.8 V. Over this interval, the ideality factor (n) ranges between 1.0 and 1.1, indicating that thermionic emission of carriers serves as the dominant current conduction mechanism in the devices under these conditions. A degradation is observed in the I–V characteristics of the devices after irradiation, with the onset of this degradation shifting from higher potentials toward lower potentials as the irradiation fluence increases. As shown in Fig. 3, at the fluences of

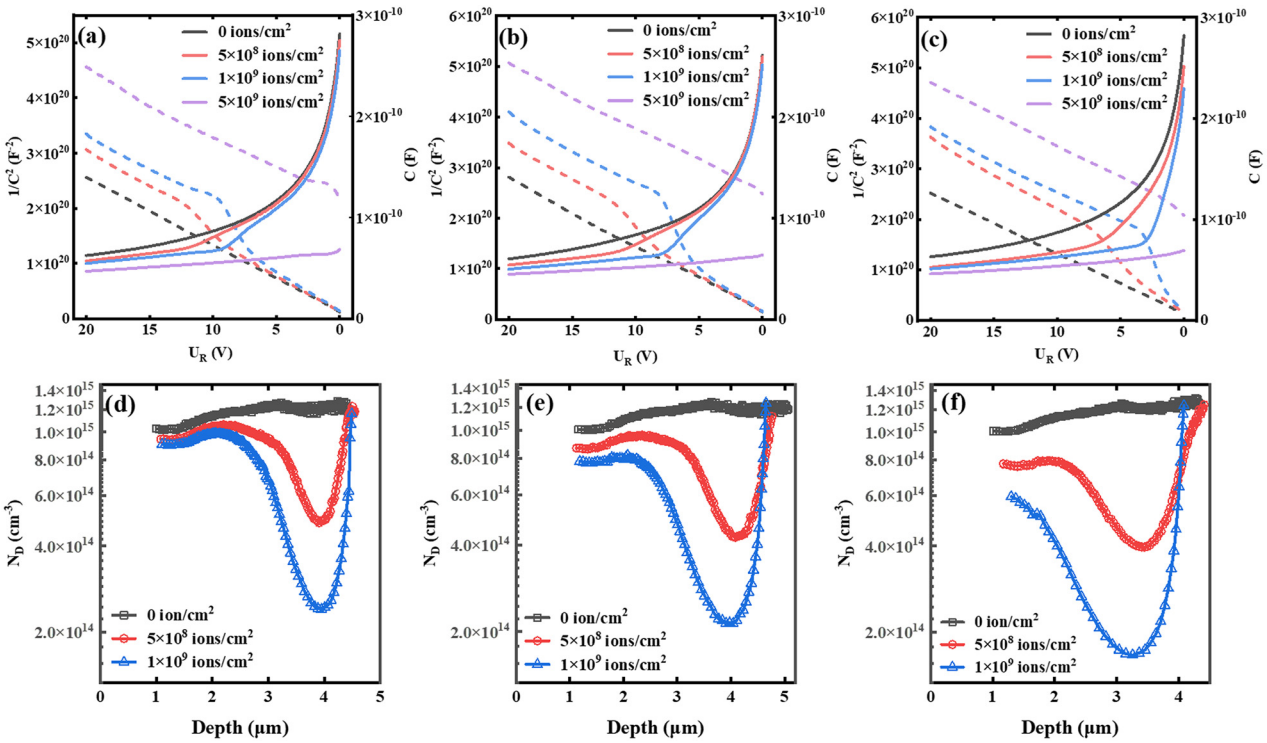

FIG. 2. C–V characteristics and the related $1/C^2$ vs reverse voltage of 4H-SiC SBD irradiated by (a) 12 MeV C, (b) 18 MeV O, and (c) 18 MeV F and depth profile of N_D for 4H-SiC SBD irradiated by (d) 12 MeV C, (e) 18 MeV O, and (f) 18 MeV F.

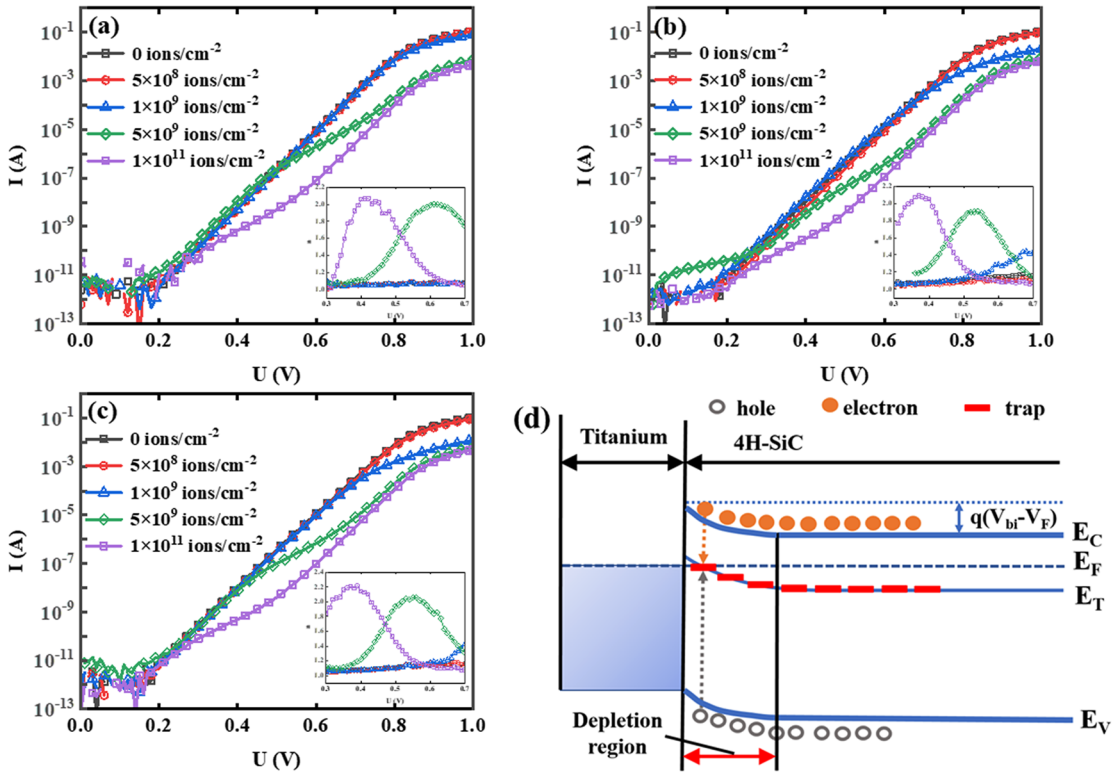

FIG. 3. Semi-logarithmic I–V characteristic of 4H-SiC SBD irradiated by (a) 12 MeV C, (b) 18 MeV O, (c) 18 MeV F, and (d) the energy band diagrams of SBD at forward bias.

5×10^8 and 1×10^9 ions/cm^2, significant degradation occurs in the high-voltage region of the I–V characteristics, while no significant change is observed in the sub-threshold region. However, as the irradiation fluence is further increased, degradation becomes apparent in the low-voltage region as well.

As is shown in Fig. 3(a), n increases from 1.07 at 0.3 V to a peak value of 2.00 at the voltage of 0.61 V irradiated by 12 MeV C with the fluence of 5×10^9 ions/cm^2. n increases from 1.01 at the voltage of 0.3 V to a peak value of 2.06 at the voltage of 0.41 V and then gradually approaches 1.05 irradiated by 12 MeV C with the fluence of 1×10^{11} ions/cm^2. According to Fig. 3(b), with the elevation of forward voltage, n increases to a peak value of 1.91 at the voltage of 0.54 V and then gradually approaches 1.08 irradiated by 18 MeV O with the fluence of 5×10^9 ions/cm^2, and n increases to a peak value of 2.09 at the voltage of 0.37 V and then gradually approaches 1.08 irradiated by 18 MeV O with the fluence of 1×10^{11} ions/cm^2. According to Fig. 3(c), with the elevation of forward voltage, n increases from 1.09 at the voltage of 0.3 to a peak value of 2.06 at the voltage of 0.55 V and then gradually approaches 1.08 irradiated by 18 MeV F with the fluence of 5×10^9 ions/cm^2, n increases to a peak value of 2.21 at the voltage of 0.39 V and then gradually approaches 1.08 irradiated by 18 MeV F with the fluence of 1×10^{11} ions/cm^2.

The degradation of I–V characteristics in the linear region under low fluence is primarily attributed to increased series resistance, resulting from the reduction of carrier concentration in the epitaxial layer. This phenomenon occurs because displacement damage induced by heavy ion irradiation predominantly localizes 3–4 μm from the Schottky contact interface, where near-interface trap concentrations remain relatively low. As presented in Fig. 3(d), at elevated fluence levels, deep level traps near the interface generate significant SRH recombination currents ($n \approx 2$) through carrier capture of both electrons and holes. When interface trap densities are low, elevated biases are required to position the Fermi level at the trap energy, necessitating higher triggering voltages for SRH recombination currents. However, increased trap concentrations enable substantial electron trap occupation even with small Fermi level shifts induced by bias, consequently activating SRH recombination currents at low voltages.

Heavy ion irradiations induced a large variety of defects, and the dominant defects in 4H-SiC have acceptor-like states in the upper part of the bandgap, which lead to the removal of free carriers with increasing irradiation fluence. To get a deeper insight into the defects in the SBDs, DLTS measurements were performed in the temperature range from 150 to 310 K with $U_P = 0$ V and $t_P = 10$ ms; the period width (T_W) was set as 4.096 s and the reverse bias voltage (U_R) was set as −20 V. Figure 4 shows the DLTS spectrum of SBD with the heavy ion irradiations; clearly, there are three deep levels in the irradiated samples. The energy level is located at E_C-0.63 eV and labeled as the $Z_{1/2}$ center, which has already been reported in numerous studies. The additional peak in the low temperature flank of $Z_{1/2}$ is labeled as E_{T1}, which is assigned to a kind of complex defect with low thermal stability.[39,41,47] There are two levels detected in the pre-irradiated sample labeled as E'_T and E''_T located at E_C - 0.51 and E_C - 0.58 eV, respectively.

The level $Z_{1/2}$ dominates the spectra at room temperature, which has been attributed to the charge transition level (0/-2) of V_C.[42–44] The

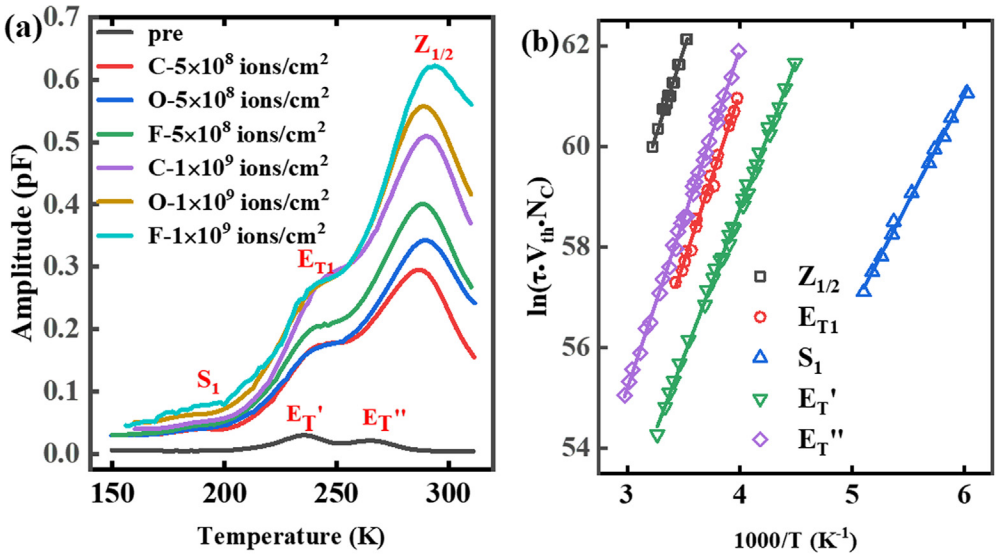

FIG. 4. (a) DLTS spectrum for irradiated 4H-SBD, (b) Arrhenius plots of $\ln(\tau \cdot V_{th} \cdot N_C)$ vs reciprocal temperature for the S_1 center, the E_T' center, the E_T'' center, the E_{T1} center, and the $Z_{1/2}$ center.

S_1 center has been identified as the charge transition level (-2/-3) of the silicon vacancy (V_{Si}).[18,45,46] Recently, the assignment of the E_{T1} to the C-related defects was strengthened by combining the density functional calculation (DFT) and the experiments.[44,46,47] The E_T' and E_T'' were observed only in unirradiated samples and exhibit good thermal stability,[48] which are identified as intrinsic defects related to interstitial atoms. The trap transition levels are summarized in Table I.

To investigate the depth profiles of electron traps generated during the irradiation, the profile scanning was implemented by changing the filling pulse voltage with a fixed reverse voltage at 300 K. Figure 5(d) shows the band diagrams of the 4H-SiC SBD; when the two filling pulse voltages U_{Pi} and U_{Pj} are applied with constant reverse voltage U_R, the trap concentration in the space charge region (the red region) is determined by the difference of transient amplitude between U_{Pi} and U_{Pj}. Depth profile of N_T is presented in the following equations:

$$N_T(x_{ji}) = \frac{2\overline{N}_D \varepsilon^2 A^2}{C_R^3} \frac{\Delta C_{ji}}{L_{Pj}^2 - L_{Pi}^2}, \tag{3}$$

$$x_{ji} = \frac{L_{Pj} + L_{Pi}}{2}, \tag{4}$$

$$W_{R,P} = \sqrt{\frac{2\varepsilon(U_{bi} + U_{R,P})}{q\overline{N}_D}}, \tag{5}$$

$$\lambda = \sqrt{\frac{2\varepsilon(E_F - E_T)}{q^2\overline{N}_D}}, \tag{6}$$

TABLE I. Transition level and electron capture cross sections of traps.

	E_C-E_T (eV)		σ (cm^2)	
Defect center	This work	Ref.	This work	Ref.
$Z_{1/2}$	0.63	0.64 [a], 0.68 [b], 0.67 [c]	4×10^{-15}	3×10^{-15} [a], 1×10^{-14} [b]
E_{T1}	0.57	0.45-0.58 [c], 0.58 [f]	2×10^{-16}	5×10^{-15} [f]
S_1	0.38	0.42[c], 0.39[d], 0.38[e]	3×10^{-16}	2×10^{-16} [d]
ET′	0.51	0.45[g]	5×10^{-16}	
ET″	0.58	0.52[g]	6×10^{-16}	

[a]Reference 41.
[b]Reference 42.
[c]Reference 44.
[d]Reference 18.
[e]Reference 46.
[f]Reference 47.
[g]Reference 48.

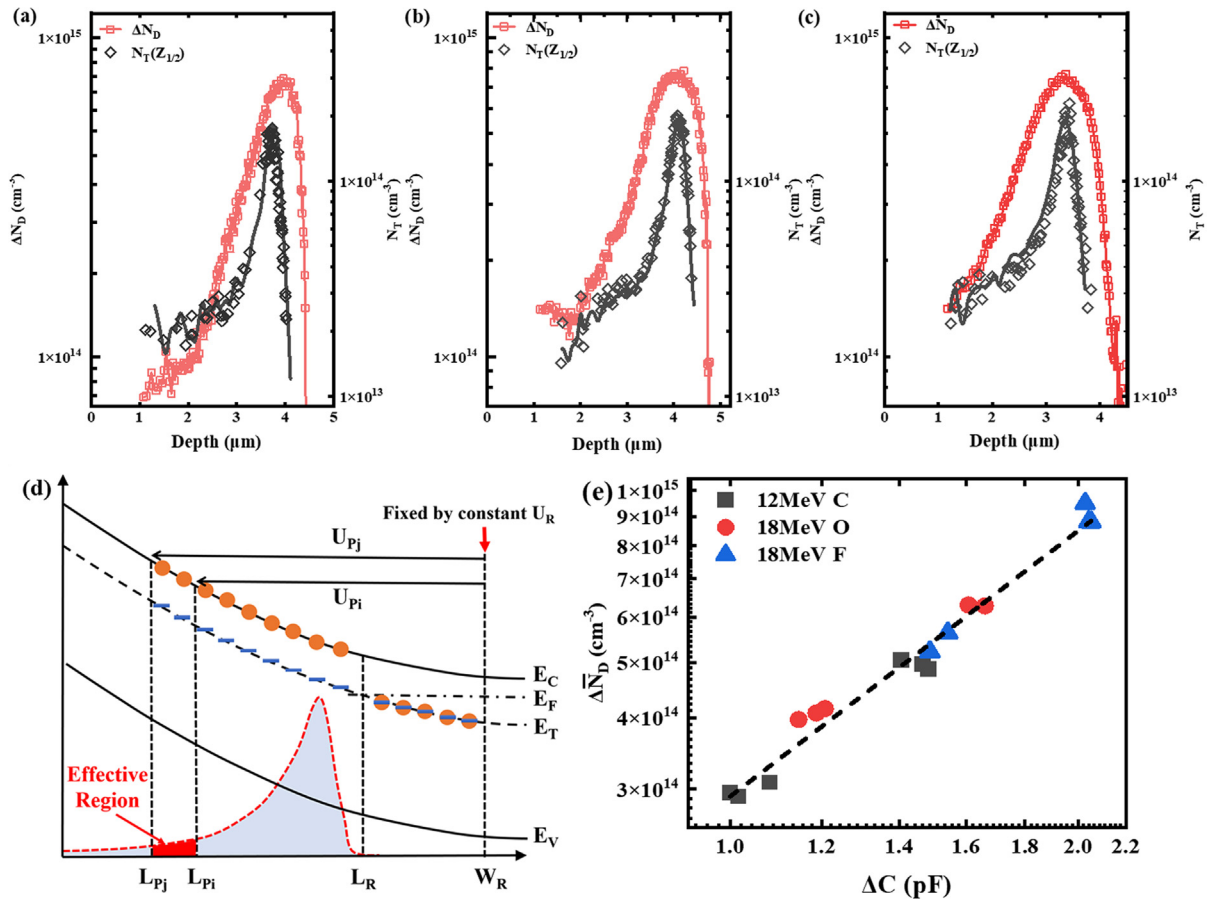

FIG. 5. Depth profiles of N_T and N_D for 4H-SiC SBDs irradiated by (a) 12 MeV C, (b) 18 MeV O, and (c) 18 MeV F with fluence at the fluence 5×10^8 ions/cm^2. (d) The band diagram of SBD when bias voltage and pulse voltage are applied for the depth profile of traps (the light blue region represents the real spatial trap distribution in the depletion region). (e) The transient amplitude (ΔC) vs ΔN_D for SBDs in the area where heavy ions are deposited.

$$L_{R,P} = W_{R,P} - \lambda, \tag{7}$$

$$\overline{N}_D = \frac{\int_{x_{start}}^{x_{end}} N_D(x)dx}{x_{end} - x_{strat}}, \tag{8}$$

where C_R is capacitance at reverse bias voltage and ΔC_{ij} is the amplitude difference of the two capacitance transients. $\overline{N}_D$ is the average carrier concentration in the region where ions are deposited. L_P and L_R are the widths of the depletion region when U_P and U_R are applied on the SBDs, x_{start} and x_{end} are the length from the start and end of the depth profile to the Schottky contact interface, respectively. E_T is the energy level of the trap and E_F is the Fermi level. The filling pulse bias voltage (U_P) was set from 0 to -20 V, the scanning step is 0.05 V, and the width of U_P was set as 10 ms. The reverse bias voltage (U_R) was set to -20 V. The depth profile of electron traps was extracted from x (L_P) = W_P-λ to a deeper region in the epitaxial layer. The results show that when the temperature is 300 K and isothermal scanning is performed with $T_w = 1.024$ s, the DLTS signal is mainly composed of $Z_{1/2}$, and the obtained result is the spatial distribution of the $Z_{1/2}$ center.

The depth profile of ΔN_D ($\Delta N_D = N_{D\text{-pre}} - N_{D\text{-irradiated}}$) and N_T is shown in Fig. 5. The blue and red lines denote the depth profiles of ΔN_D at the fluence 5×10^8 and 1×10^9 ions/cm^2, respectively. The black lines denote the depth profile of N_T at the fluence 5×10^8 ions/cm^2. Apparently, the decrease in local carrier concentration induced by ion irradiation are well consistent with the distribution of traps in the epitaxial layer. As we have discussed, the displacement damage induced by heavy ions was concentrated in the tail of the ion incidence trajectory. As is shown in Fig. 1(b), three types of heavy ions, 12 MeV C, 18 MeV O, and 18 MeV F are injected into the 4H-SiC SBD, and 18 MeV F presented the shallowest incident depth compared to 12 MeV C and 18 MeV O, SBDs irradiated by 18 MeV F present the largest NIEL in the ions deposited region. 18 MeV O presented a larger incident depth and smaller NIEL in the ion deposited region compared to 18 MeV F, which is consistent with the results calculated by ERETCAD. Compared with 18 MeV O and 18 MeV F, 12 MeV C presented the smallest NIEL and an incident depth between the two ions. In summary, 18 MeV F presents the highest average displacement damage, followed by 18 MeV O, while 12 MeV C presented the

lowest average displacement damage, which is well consistent with the results in Fig. 2.

Figures 5(a)–5(c) show the schematic comparison for depth profile of ΔN_D and N_T for SBD irradiated by three heavy ions with the fluence of $5 \times 10^8\,cm^{-2}$. It should be noted that during the extraction of the carrier concentration profile via C–V measurements, it was observed that the presence of SRH recombination leads to an underestimation of carrier concentration values near the peak of the profile. Consequently, we have selected the average carrier concentration $\Delta\overline{N}_D$ and $\overline{N}_T$ [determined by Eqs. (9) and (10)] as the assessment metric, as illustrated in Fig. 5(e). As is shown in Fig. 5(a), for the SBDs irradiated by 12 MeV C, the maximum of ΔN_D is located at $x = 3.8\,\mu m$ (depth starting from the Schottky contact interface) and $\Delta\overline{N}_D$ is $2.97 \times 10^{14}\,cm^{-3}$. Correspondingly, the maximum of $Z_{1/2}$ center $N_T(Z_{1/2})$ $(1.69 \times 10^{14}\,cm^{-3})$ is located at $x = 3.7\,\mu m$ and the $\overline{N}_T$ is $4.32 \times 10^{13}\,cm^{-3}$. As is shown in Fig. 5(b), for the SBDs irradiated by 18 MeV O, the maximum of ΔN_D is located at $x = 4.1\,\mu m$ and $\Delta\overline{N}_D$ is $3.64 \times 10^{14}\,cm^{-3}$, the maximum of N_T $(2.1 \times 10^{14}\,cm^{-3})$ is located at $x = 4.1\,\mu m$ and the $\overline{N}_T$ is $5.32 \times 10^{13}\,cm^{-3}$. As is shown in Fig. 5(c), for the SBDs irradiated by 18 MeV F, the maximum of ΔN_D is located at $x = 3.4\,\mu m$ and $\Delta\overline{N}_D$ is $4.27 \times 10^{14}\,cm^{-3}$, the maximum of N_T $(Z_{1/2})$ $(3.2 \times 10^{14}\,cm^{-3})$ is located at $x = 3.4\,\mu m$ and the $\overline{N}_T$ is $5.82 \times 10^{13}\,cm^{-3}$. All in all, the well consistent plots for the depth profile of N_T and ΔN_D obtained by using the depth profile of trap concentration calculated with the space charge region demonstrate the carrier removal effects caused by $Z_{1/2}$.

The average carrier concentration $\overline{N}_D$ was used for calculation of the depletion depth in Eq. (8). Due to the inhomogeneous distribution of the actual carrier concentration in the region where the displacement damage is concentrated, an underestimate for the trap concentration depth calculation in the region where carrier removal effects are concentrated is inevitable, which is acceptable at lower irradiation fluence. As a result, the peak width of the depth profile of ΔN_D is smaller than the depth profile of N_T, and the phenomenon increases with the increase in irradiation fluence.

In this work, the trap concentration at the tail of the ion incident track is in the same order of magnitude as the carrier concentration of the SBDs, the conventional calculation of trap concentration is no longer applicable. The transient amplitude (ΔC) was used to evaluate the carrier removal effect for the irradiated sample. According to the analysis of the depth profile of trap concentration, ΔC was measured in the region where the ions deposited by adjusting the U_P and U_R. The average value of ΔN_D and $\overline{N}_T$ is determined by the following equations:

$$\Delta\overline{N}_D = \frac{\int_{x_{start}}^{x_{end}} \Delta N_D(x)dx}{x_{end} - x_{strat}}, \tag{9}$$

$$\overline{N}_T = \frac{\int_{x_{start}}^{x_{end}} N_T(x)dx}{x_{end} - x_{strat}}. \tag{10}$$

Figure 5(e) shows the trap concentration vs the average carrier concentration for all the samples. Clearly, in the region where the heavy ions were deposited, a well linear relationship can be observed between $\Delta\overline{N}_D$ and N_T.

In conclusion, this work analyzed the displacement damage of the heavy ion irradiation effects on 4H-SiC SBD, including the degradation of free carrier concentration and the generation of defects through C–V and DLTS measurements. The concentrated distribution of displacement energy loss at the tail end of the ion range leads to irregular degradation of the C–V curve, accompanied by a severe carrier removal effect. Three deep levels were observed in the bandgap induced by 12 MeV C, 18 MeV O, and 18 MeV F, including the $Z_{1/2}$ center, the E_{T1} center, and the S_1 center. Depth profile of traps characterized by isothermal transient measurements by scanning the filling pulse voltage with a fixed reverse bias voltage; the method was utilized to investigate the spatial distribution of defects in 4H-SiC SBD. The results suggest that the inhomogeneous distribution of acceptor defects leads to anomalous doping profiles. This work provides support for the characterization of 4H-SiC defects and the evaluation of displacement damage. The methods used in this work also enable the characterization of trap depth distribution applicable in other semiconductor devices.

See the supplementary material for a degradation comparison of the electrical performance of the device at bias voltages of −200 and 0 V, DLTS spectra, and depth distribution of traps. The results indicate that the electric field in this work has no significant impact on the types and distribution of traps in 4H-SiC SBD.

This work is sponsored by the State Key Laboratory of Space Environment Interaction with Matters.

AUTHOR DECLARATIONS

Conflict of Interest

The authors have no conflicts to disclose.

Author Contributions

Xueqiang Yu: Conceptualization (equal); Data curation (equal); Formal analysis (equal); Funding acquisition (equal); Investigation (equal); Methodology (equal); Project administration (equal); Software (equal); Writing – original draft (equal); Writing – review & editing (equal). **Xiaodong Xu:** Conceptualization (equal); Data curation (equal); Formal analysis (equal); Funding acquisition (equal); Project administration (equal); Software (equal); Supervision (equal); Visualization (equal); Writing – original draft (equal); Writing – review & editing (equal). **Hao Jiang:** Data curation (equal); Formal analysis (equal); Software (equal); Supervision (equal); Validation (equal); Visualization (equal); Writing – review & editing (equal). **Lei Wu:** Conceptualization (equal); Data curation (equal); Methodology (equal). **Fengkai Liu:** Data curation (equal); Methodology (equal); Software (equal). **Weiqi Li:** Conceptualization (equal); Methodology (equal); Supervision (equal); Validation (equal); Visualization (equal); Writing – review & editing (equal). **Zhongli Liu:** Conceptualization (equal); Data curation (equal); Software (equal); Writing – review & editing (equal). **Hongbin Geng:** Conceptualization (equal); Funding acquisition (equal); Methodology (equal); Supervision (equal). **Jianqun Yang:** Conceptualization (equal); Funding acquisition (equal); Investigation (equal); Resources (equal); Supervision (equal). **Xingji Li:** Conceptualization (equal); Investigation (equal); Methodology (equal); Project administration (equal); Supervision (equal); Visualization (equal); Writing – original draft (equal).

DATA AVAILABILITY

The data that support the findings of this study are available from the corresponding authors upon reasonable request.

REFERENCES

[1]J. Y. Lee, S. Singh, and J. A. Cooper, IEEE Trans. Electron Devices **55**(8), 1946 (2008).
[2]F. Zhao, M. M. Islam, P. Muzykov, A. Bolotnikov, and T. S. Sudarshan, IEEE Electron Device Lett. **30**(11), 1182 (2009).
[3]P. G. Neudeck, D. J. Spry, L. Chen, N. F. Prokop, and M. J. Krasowski, IEEE Electron Device Lett. **38**(8), 1082 (2017).
[4]J. A. McPherson, C. W. Hitchcock, T. Paul Chow, W. Ji, and A. A. Woodworth, IEEE Trans. Nucl. Sci. **68**(5), 651 (2021).
[5]A. Metreveli, A. Hallén, I. D. Sarcina, A. Cemmi, J. Scifo, A. Verna, and C. M. Zetterling, IEEE Trans. Nucl. Sci. **70**(12), 2597 (2023).
[6]D. T. Morisette, J. A. Cooper, M. R. Melloch, G. M. Dolny, P. M. Shenoy, M. Zafrani, and J. Gladish, IEEE Trans. Electron Devices **48**(2), 349 (2001).
[7]C. H. Yu, Y. Wang, M. T. Bao, X. J. Li, J. Q. Yang, and Z. H. Tang, IEEE Trans. Electron Devices **68**(7), 3711 (2021).
[8]Y. Tang, L. Wang, X. Cai, D. Hu, B. Dong, L. Ding, Y. Gao, R. Xia, M. Gao, S. Wang, J. Dang, F. Zhao, and B. Li, IEEE Trans. Nucl. Sci. **70**(8), 1990 (2023).
[9]S. Yang, X. Liang, J. Cui, Q. Zheng, J. Sun, M. Liu, D. Zhang, H. Feng, X. Yu, C. Xiang, Y. Li, and Q. Guo, J. Semicond. **42**(8), 082802 (2021); X. Li, J. Yang, C. Liu, P. Li, Y. Zhao, and G. Liu, IEEE Trans. Nucl. Sci. **64**(3), 976 (2017).
[10]C. Liu, X. Zhang, J. Yang, X. Li, and G. Ma, Nucl. Instrum. Methods Phys. Res., Sect. B **409**, 246 (2017).
[11]X. Li, C. Liu, M. Lan, L. Xiao, J. Liu, D. Ding, D. Yang, and S. He, Nucl. Instrum. Methods Phys. Res., Sect. A **716**, 10 (2013).
[12]F. Liu, Z. Liu, X. Jin, S. Liu, L. Wu, J. Yang, J. Luo, R. Xu, and X. Li, IEEE Trans. Nucl. Sci. **71**(8), 1989 (2024).
[13]L. Wu, S. Dong, F. Liu, Z. Liu, Y. Wei, W. Li, X. Xu, J. Yang, and X. Li, IEEE Trans. Nucl. Sci. **71**(7), 1370 (2024).
[14]J. R. Srour, C. J. Marshall, and P. W. Marshall, IEEE Trans. Nucl. Sci. **50**(3), 653 (2003).
[15]S. S. Suvanam, S. I. Kuroki, L. Lanni, R. Hadayati, T. Ohshima, T. Makino, A. Hallén, and C. M. Zetterling, IEEE Trans. Nucl. Sci. **64**(2), 852 (2017).
[16]A. Mihaila, L. Knoll, E. Bianda, M. Bellini, S. Wirths, G. Alfieri, L. Kranz, F. Canales, and M. Rahimo, paper presented at the IEEE International Electron Devices Meeting (IEDM), 2018.
[17]E. Omotoso, W. E. Meyer, P. J. Janse van Rensburg, E. Igumbor, S. M. Tunhuma, P. N. M. Ngoepe, H. T. Danga, and F. D. Auret, Nucl. Instrum. Methods Phys. Res, Sect. B **409**, 241 (2017).
[18]E. Omotoso, W. E. Meyer, F. D. Auret, A. T. Paradzah, and M. J. Legodi, Nucl. Instrum. Methods Phys. Res., Sect. B **371**, 312 (2016).
[19]L. Zhiyun, C. Tianbing, A. C. Ahyi, A. K. Sutton, B. M. Haugerud, J. D. Cressler, D. C. Sheridan, J. R. Williams, P. W. Marshall, and R. A. Reed, IEEE Trans. Nucl. Sci. **51**(6), 3748 (2004).
[20]F. Moscatelli, A. Scorzoni, A. Poggi, M. Bruzzi, S. Sciortino, S. Lagomarsino, G. Wagner, I. Mandic, and R. Nipoti, IEEE Trans. Nucl. Sci. **53**(3), 1557 (2006).
[21]X. Xu, X. Yu, J. Yang, T. Ying, X. Cui, Y. Jing, G. Lv, Z. Liu, W. Li, and X. Li, Comput. Mater. Sci. **215**, 111760 (2022).
[22]H. Lefevre and M. Schulz, IEEE Trans. Electron Devices **24**, 973 (1977).
[23]N. M. Johnson, D. J. Bartelink, R. B. Gold, and J. F. Gibbons, J. Appl. Phys. **50**(7), 4828 (1979).
[24]K. Kawahara, G. Alfieri, and T. Kimoto, J. Appl. Phys. **106**(1), 013719 (2009).
[25]K. Kanegae, T. Okuda, M. Horita, J. Suda, and T. Kimoto, J. Appl. Phys. **130**(10), 105703 (2021).
[26]S. Kozakai, H. Fujii, M. Kaneko, and T. Kimoto, J. Appl. Phys. **136**(9), 095702 (2024).
[27]J. Zhang, L. Storasta, J. P. Bergman, N. T. Son, and E. Janzén, J. Appl. Phys. **93**(8), 4708 (2003).
[28]P. B. Klein, B. V. Shanabrook, S. W. Huh, A. Y. Polyakov, M. Skowronski, J. J. Sumakeris, and M. J. O'Loughlin, Appl. Phys. Lett. **88**(5), 052110 (2006).
[29]L. Storasta and H. Tsuchida, Appl. Phys. Lett. **90**(6), 062116 (2007).
[30]L. Storasta, H. Tsuchida, T. Miyazawa, and T. Ohshima, J. Appl. Phys. **103**(1), 013705 (2008).
[31]J. Coutinho, V. J. B. Torres, K. Demmouche, K. Demmouche, and S. Öberg, Phys. Rev. B **96**, 174105 (2017).
[32]P. Dong, X. Yan, L. Zhang, S. Jin, F. Dai, Y. Zhang, Y. Cui, X. Yu, and B. Huang, IEEE Trans. Nucl. Sci. **68**(3), 312 (2021).
[33]D.-S. Chao, H.-Y. Shih, J.-Y. Jiang, C.-F. Huang, C.-Y. Chiang, C.-S. Ku, C.-T. Yen, L.-S. Lee, F.-J. Hsu, K.-T. Chu, C.-C. Hung, and C.-Y. Lee, Jpn. J. Appl. Phys., Part 1 **58**(SB), SBBD08 (2019).
[34]J. Yang, H. Li, S. Dong, and X. Li, IEEE Trans. Nucl. Sci. **66**(9), 2042 (2019).
[35]A. Castaldini, A. Cavallini, L. Rigutti, F. Nava, S. Ferrero, and F. Giorgis, J. Appl. Phys. **98**(5), 053706 (2005).
[36]I. Capan, T. Brodar, T. Makino, V. Radulovic, and L. Snoj, Crystals **11**(11), 1404 (2021).
[37]P. Hazdra and S. Popelka, IET Power Electron. **12**(15), 3910 (2019).
[38]Z. P. Wang, H. H. Gong, X. X. Yu, T. C. Hu, X. L. Ji, F.-F. Ren, S. L. Gu, Y. D. Zheng, R. Zhang, and J. D. Ye, Appl. Phys. Lett. **122**, 152102 (2023).
[39]I. Capan, T. Brodar, Ž. Pastuović, R. Siegele, T. Ohshima, S.-I. Sato, T. Makino, L. Snoj, V. Radulović, J. Coutinho, V. J. B. Torres, and K. Demmouche, J. Appl. Phys. **123**, 161597 (2018).
[40]H. Li, Y. Jing, X. Xu, H. Jiang, J. Zhao, Y. Sun, W. Li, J. Yan, J. Yang, and X. Li, Nucl. Instrum. Methods Phys. Res., Sect. B **550**, 165313 (2024).
[41]Ž. Pastuović, R. Siegele, I. Capan, T. Brodar, S-i Sato, and T. Ohshima, J. Phys. **29**, 475701 (2017).
[42]T. Brodar, I. Capan, V. Radulović, L. Snoj, Ž. Pastuović, J. Coutinho, and T. Ohshima, Nucl. Instrum. Methods Phys. Res., Sect. B **437**, 27 (2018).
[43]N. T. Son, X. T. Trinh, L. S. Løvlie, B. G. Svensson, K. Kawahara, J. Suda, T. Kimoto, T. Umeda, J. Isoya, T. Makino, T. Ohshima, and E. Janzén, Phys. Rev. Lett. **109**(18), 187603 (2012).
[44]R. Karsthof, M. E. Bathen, A. Galeckas, and L. Vines, Phys. Rev. B **102**(18), 184111 (2020).
[45]M. E. Bathen, A. Galeckas, J. Müting, H. M. Ayedh, U. Grossner, J. Coutinho, Y. K. Frodason, and L. Vines, npj Quantum Inf. **5**(1), 111 (2019).
[46]X. Yu, X. Xu, H. Jiang, Y. Wei, T. Ying, W. Li, G. Lv, H. Geng, Y. Huang, Z. Liu, J. Yang, and X. Li, Comput. Mater. Sci. **246**, 113365 (2025).
[47]M. E. Bathen, R. Karsthof, A. Galeckas, P. Kumar, A. Y. Kuznetsov, U. Grossner, and L. Vines, Mater. Sci. Semicond. Process. **176**, 108316 (2024).
[48]C. G. Hemmingsson, N. T. Son, A. Ellison, J. Zhang, and E. Janzén, Phys. Rev. B **58**(16), R10119 (1998).